This article has been accepted for publication in a future issue of this journal, but has not been fully edited. Content may change prior to final publication. Citation information: DOI 10.1109/TPEL.2018.2823426, IEEE Transactions on Power Electronics

PV System Control to Provide Active Power Reserves under Partial Shading Conditions

Efstratios I. Batzelis, *Member, IEEE,* Stavros A. Papathanassiou, *Senior Member, IEEE,* and Bikash C. Pal, *Fellow, IEEE*

***Abstract*—The challenges of modern power systems will inevitably impose increased ancillary service requirements to photovoltaic (PV) plants in the future, including operating reserves. Recent studies investigate methods to maintain active power reserves without energy storage in the standard case of uniform illumination. In this paper, this functionality is extended to partial shading conditions, often encountered in PV systems. A new control scheme is proposed that permits operation at a reduced power level, estimating at the same time the shading conditions and maximum available power. This is achieved by applying a least squares curve fitting algorithm on voltage and current measurements, without relying on any irradiance or temperature sensors. To the best of our knowledge, this is the first power reserves control scheme for PV systems under partial shading presented in the literature. The robustness and effectiveness of the proposed method is validated under rapidly changing shading conditions through simulations and experimental tests on a 2 kW PV system prototype.**

***Index Terms*—Active power control, maximum power point tracking (MPPT), partial shading, power reserves, photovoltaic (PV) system.**

I. Introduction

THE The intermittent nature of renewable energy generation imposes technical challenges to the power system operation and control [1], [2]. Network codes are constantly revised, requiring increasingly more services from these systems, including fault-ride-through, reactive power injection, frequency response, operating reserves and output power variability (rate of change) constraints [3]–[9]. To provide some of these services, a power plant should be able to keep active power reserves and track power set-points, permitting effective up and down regulation of its output on command [10]–[12].

In photovoltaic (PV) systems, operating reserves can be provided by either installing energy storage or curtailing generation [5], [12]–[14]. The former option employs batteries [15] ultra capacitors [16] or fuel cells [17] to reutilize the curtailed energy, albeit at an increased installation and maintenance cost. The latter approach involves wasting available energy but is easily implemented using a dump load [18] or, more frequently, by modifying the maximum power point tracking (MPPT) algorithm to operate at a reduced power level [1], [4], [6], [11]–[13], [19]–[25]. This control-based alternative has attracted the interest of researchers lately, as it requires no additional hardware and is therefore considered a cost-effective solution [11]–[13]. Major challenges in implementing these methods include: a) effectively tracking power set-points in dynamic conditions and b) monitoring the maximum power while it changes over time [13].

In order to extend the power reserves requirement to small and medium scale PV plants, where a two-stage string-inverter topology is most often adopted [11], [12], modification of the dc/dc converter control is required [10]. In [11], [12], [19]–[21], MPPT-like control schemes are proposed that involve perturbation of the operating point in discrete voltage steps, thus exhibiting mediocre dynamic response. For a better response, a voltage PI controller is employed in [10], [26], which however proves ineffective in tracking power set-points. To address this issue, a control scheme that involves modification of the P-V curve is presented in [13], which enables direct regulation of the power, rather than the voltage. However, all these studies assume uniform illumination and are not suitable for partial shading conditions.

Furthermore, estimation of the available power is a challenging but important task that allows to keep track of maintained reserves [11]–[13]. In [1], [6], [22], [23], this estimation is performed by means of irradiance/temperature sensors and a mathematical model; although simple, this approach suffers in accuracy due to the inevitable deviations of the actual PV system parameters from datasheet values [11]–[13]. The method presented in [12] requires that a part of the PV plant operates in MPPT mode to monitor the actual maximum power; yet, this approach is suitable only for large PV plants with identical components and conditions. An interesting alternative is proposed in [11], where the system periodically enters MPPT mode, the excess energy being stored in the dc link, thus not affecting the grid-side output; however, increasing the dc link voltage close to its upper limit raises safety concerns. In [10], [13], [21], [24]–[26], a mathematical model is applied on voltage and current measurements to estimate the maximum power: simplified linear/quadratic models are applied on a few samples in [10], [21], [25], while curve fitting algorithms based on the single-diode PV model are employed in [13], [24] to tackle problems caused by noise. Among all aforementioned studies, partial shading conditions are taken

Manuscript received November 14, 2017; revised January 30, 2018 and March 8, 2018; accepted March 21, 2018. Dr. E. Batzelis work has received funding from the European Unions Horizon 2020 research and innovation programme under the Marie Sklodowska-Curie grant agreement No 746638. Prof. B. Pals work has been conducted as part of the research project Joint UK-India Clean Energy Centre (JUICE) which is funded by the RCUK's Energy Programme (contract no: EP/P003605/1). Paper no. TPEL-Reg-2017-11-2170.

E. I. Batzelis and B. C. Pal are with the Department of Electrical and Electronic Engineering, Imperial College London, London SW7 2AZ, UK (e-mail: e.batzelis@imperial.ac.uk; b.pal@imperial.ac.uk).

S.A. Papathanassiou is with the School of Electrical and Computer Engineering, National Technical University of Athens, Athens 15780, Greece (e-mail: st@power.ece.ntua.gr).

This article has been accepted for publication in a future issue of this journal, but has not been fully edited. Content may change prior to final publication. Citation information: DOI 10.1109/TPEL.2018.2823426, IEEE Transactions on Power Electronics

into account only in [1] for microinverter systems; yet, this technique is not applicable to the string-inverter topology, where partial shading gives rise to multiple power peaks on the P-V curve [27]–[29].

In light of these limitations, a power reserves control scheme for two-stage PV systems is proposed in this paper, especially designed for *partial shading conditions*. A special modification of the multi-peak P-V curve is introduced that allows adoption of a power PI controller to quickly and effectively track *power set-points*. Furthermore, a new method is proposed to *estimate the maximum power* while keeping reserves. A least-squares curve fitting algorithm is applied on voltage and current measurements using the PV models derived in [27], [29]–[31] to determine the shading conditions, the MPPs and the entire P-V curve *in real-time*. This is achieved by slightly perturbing the operating point around the power reference to generate the necessary input data for successful curve fitting; there is no need for periodic MPPT operation, as done in other studies. To the best of our knowledge, this is the first method to provide these estimations from a curtailed power level *under partial shading* in a purely mathematical way. The proposed control is essentially an improvement of [13] utilizing findings of [31] to permit application under partial shading; the algorithm is developed for PV strings (series-connected modules) illuminated at two different irradiance levels and does not require any additional hardware, such as irradiance or temperature sensors. The reliable and effective operation is validated through simulations in MATLAB/Simulink and experimental tests on a 2 kW PV system operating under very fast-changing shading conditions. The proposed method is an easy way to render a PV system without storage a dispatchable power plant, being able to provide reserves and other ancillary services, such as frequency regulation, to the grid.

The proposed control scheme is described in Section II, followed by the MPPs estimation algorithm in Section III. Simulation and experimental results are discussed in Sections IV and V respectively, while the circuit equations adopted are briefly given in the Appendix.

II. Power Reserves Control for Partial Shading

The configuration of a two-stage PV inverter is depicted in Fig. 1. The dc/dc converter, usually a boost converter, regulates the operating point and extracts the power from the PV generator adjusting the duty cycle D_{conv}. The inverter transfers that amount of energy to the grid and maintains a constant dc link voltage by applying a P-Q control algorithm [11], [13], [32].

Conventionally, the control of the dc/dc converter is done through a simple MPPT algorithm. To allow operation at a reduced power level, however, a more sophisticated control scheme is presented in this section, which incorporates five individual subsystems highlighted in colour in Fig. 1. The *Reserves* module determines the scheduled power P_{sch} based on a reserves command; this constitutes the power reference P_{pvref} that the Main control module tracks by regulating the duty cycle D_{main}. The maximum power is continuously estimated by the *MPPs estimator* block using voltage and

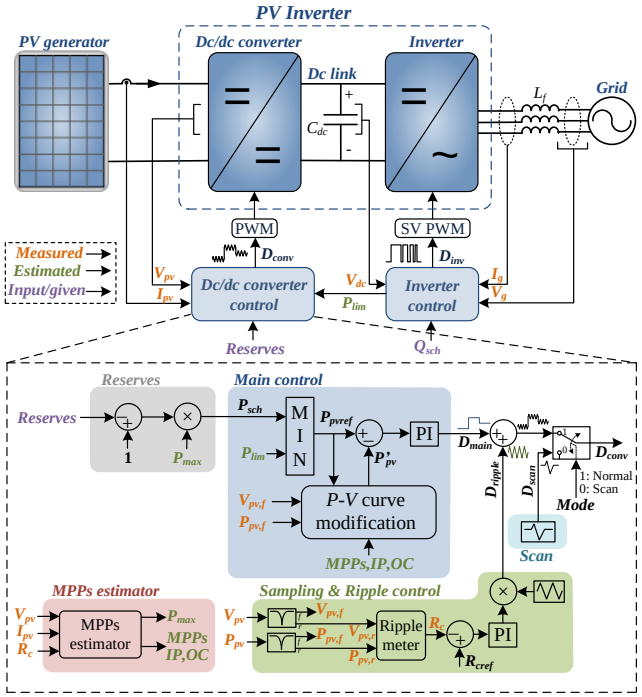

Fig. 1. Topology of a two-stage PV system and proposed control scheme.

current measurements at the PV side. To ensure these measurements are fit for purpose, the *Sampling & Ripple control* subsystem introduces a perturbation signal D_{ripple} to create limited oscillation of the operating point. When the shadow first appears, a quick curve scan is performed by the Scan block by varying the duty cycle D_{scan}. The final duty cycle of the converter, D_{conv}, will be either $(D_{main} + D_{ripple})$ or D_{scan}, depending on the operating Mode. In the following, these modules are described in detail.

A. Reserves Module

The requested reserves may correspond to a command issued by the grid operator or to the output of an internal control block. Reserves may be either a specific power level (kW) [6], [11], [12], [23] or a fraction of available power P_{max} [1], [10], [13], [22], [24], [26]. The latter approach is adopted in Fig. 1, as it better reflects the grid codes requirements, e.g. [3]:

$$P_{sch} = (1 - Reserves)P_{max} \tag{1}$$

where *Reserves* may range from 0 to 1. Alternatively, a direct power set-point P_{req} can be imposed, upper bounded by P_{max}:

$$P_{sch} = \min\{P_{req}, P_{max}\} \tag{2}$$

Notably, both approaches need the maximum power P_{max}.

B. Main Control Module

Objective of this subsystem is to regulate the duty cycle D_{main} in order to track a power reference P_{pvref}, based on

This article has been accepted for publication in a future issue of this journal, but has not been fully edited. Content may change prior to final publication. Citation information: DOI 10.1109/TPEL.2018.2823426, IEEE Transactions on Power Electronics

P_{sch} after applying a power limit P_{lim} (set by the inverter control to contain the transferred power during faults [33]):

$$P_{pvref} = \min\{P_{sch}, P_{lim}\} \tag{3}$$

As explained in [13], to permit regulation to this power reference, a single voltage regulator is not sufficient. A need for extra control loops or MPPT-like control arises that may have a negative impact on the dynamic response and stability of the system. This study adopts and expands the concept of [13], where a power PI controller is used to regulate a *modified PV power signal*, P'_{pv}, to the reference P_{pvref} (Fig. 1). This modification is necessary to establish a monotonic relation between the input (power) and output (duty cycle) of the PI controller, as established in [13] for uniform illumination. It is worth noting that this approach ignores the power conversion losses, which are typically very small; as a result, the actual reserves maintained may be slightly less that the requested value. If extra high reserves accuracy is required, this deviation can be compensated considering the converter efficiency, as explained in [11].

1) Reserves under partial shading: Under partial shading conditions the *P-V* curve becomes more complicated and proper modification is quite challenging. An indicative shading scenario is illustrated in Fig. 2, with 2 out of 12 modules of a PV string being shaded (Fig. 2(a)). The respective *P-V* curve is shown in Fig. 2(b), indicating the uphill (blue line) and downhill (green line) sections. Two local maxima appear: *MPP1* and *MPP2*; the values of these MPPs depend on the shading conditions and either of them may be the global maximum (MPP1 in Fig. 2(b)). Other important operating points are the inflection point (IP - [34], [35]) and the open circuit point (OC); MPP1, MPP2, IP and OC are hereafter referred to as the *key operating points*. For a given power reference (purple dotted line), there exist up to four possible operating points (Op1-Op4); selecting the most appropriate is not a trivial task.

There is a debate in the literature about the preferable operating region at reduced power, between the right or left-hand side of the *P-V* curve (for the uniform illumination case). While the former benefits from improved converter efficiency [11], [25], faster dynamic response [21], [22] and no limit on the level of reserves [13], [21], the latter provides increased robustness under fast irradiance variation [11], [12]. Yet, at two different irradiance levels there are four possible operating regions, rather than two (Fig. 2(b)). Depending on the shading conditions, Op1 on the *leftmost uphill* section may correspond to very low voltage, while Op3 on the *rightmost uphill* section may be valid only for a limited power range. On the other hand, the *downhill* sections (green lines - Op2 and Op4) benefit from the aforementioned advantages of the right-hand side of the *P-V* curve. Therefore, in this study the *downhill* sections are considered preferable under partial shading conditions.

2) Modification of the P-V curve (two irradiance levels): As discussed above, there is a need to derive a monotonic version of the *P-V* curve in order to apply a power PI controller. To include both downhill sections in this modification, two individual curves P_{mod1} and P_{mod2} are introduced (coloured dashed lines in Fig. 3). Essentially, each of these curves correspond to one downhill section extended by descending linear segments using the key operating points:

$$P_{mod1} = \begin{cases} -\frac{P_{mp1}(V-V_{mp1})}{V_{mp1}} + P_{mp1} & , V < V_{mp1} \\ P & , V_{mp1} \le V \le V_{ip} \\ -\frac{P_{ip}(V-V_{oc})}{V_{ip}-V_{oc}} & , V > V_{ip} \end{cases} \tag{4}$$

$$P_{mod2} = \begin{cases} -\frac{P_{mp2}(V-V_{mp2})}{V_{mp2}} + P_{mp2} & , V < V_{mp2} \\ P & , V \ge V_{mp2} \end{cases} \tag{5}$$

The final modified power feedback, P'_{pv}, fed into the PI controller will be either P_{mod1} or P_{mod2} according to the selection rule:

$$P'_{pv} = \begin{cases} P_{mod1} & , (P_{ref} > P_{mp2}) \text{ or } (P_{mp1} > P_{mp2} \\ & \quad \text{and } P_{ref} > P_{ip} \text{ and } V < V_{ip}) \\ P_{mod2} & , \text{otherwise} \end{cases} \tag{6}$$

This is graphically illustrated in Fig. 3. If P_{ref} lies only in one downhill section ($P_{ref} > P_{mp2}$ or $P_{ref} < P_{ip}$), the modified curve that corresponds to that section is assigned to P'_{pv} (vertical green or red arrow respectively in Fig. 3); if, however, P_{ref} lies in both downhill sections ($P_{ip} < P_{ref} < P_{mp2}$), the modified curve that already contains the operating point is selected, comparing the voltage V_{pv} to the IP voltage V_{ip}

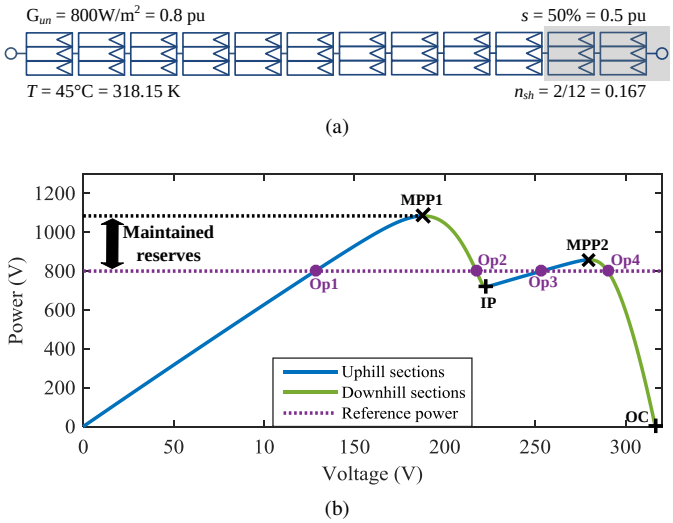

Fig. 2. (a) Indicative scenario of partially shaded operation of a PV string. (b) *P-V* curve with two MPPs and requested reserves level.

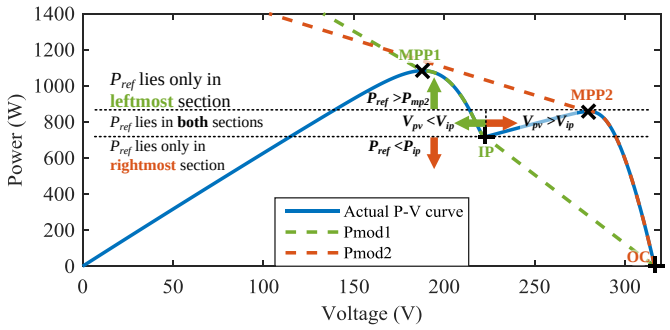

Fig. 3. Modification of the *P-V* curve under partial shading.

This article has been accepted for publication in a future issue of this journal, but has not been fully edited. Content may change prior to final publication. Citation information: DOI 10.1109/TPEL.2018.2823426, IEEE Transactions on Power Electronics

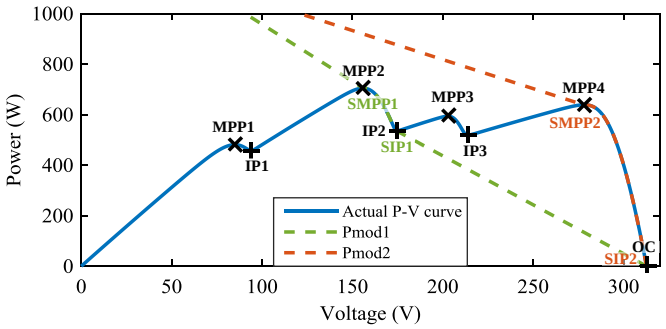

Fig. 4. Modification of multi-peak *P-V* curves.

(horizontal green (P_{mod1}) or red (P_{mod2}) arrow in Fig. 3). This way, a small deadband is established which prevents unnecessary transition of the operating point from one section to another. Combining (4)-(6), a monotonic relation between the input and output of the PI controller of the Main control module is established (Fig. 1).

3) Modification of multi-peak P-V curves: In this section, it is shown how the modification rule can be extended to the general case of multi-peak *P-V* curves. To facilitate understanding, the indicative case of Fig. 4 is used as an example: there are four MPPs (MPP1-MPP4), three IPs (IP1-IP3) and several possible operating points for a given power reference. Based on the previous discussion, the most preferable operating region lies in the *rightmost downhill section* that provides the required P_{ref}.

However, there is no need to consider all downhill segments in the modification, since a subset of those may suffice for all possible P_{ref} values (e.g. MPP2-IP2 and MPP4-OC sections in Fig. 4). In the general multi-peak case, one has to find the *minimum subset of rightmost downhill sections* that collectively provide the entire power range; these sections are defined by their bounds: *subset of MPPs* (SMPPs) and *subset of IPs* (SIPs). The flowchart of this process is illustrated in Fig. 5(a), where *n* and *m* are the total number of MPPs and SMPPs respectively. In Fig. 4, this algorithm results in SMPP1, SMPP2 and SIP1, SIP2.

Thereafter, a modified curve is assigned to each one of the selected sections depending on the SMPP*i* = $(V_{smp\text{-}i}, P_{smp\text{-}i})$ and SIP*i* = $(V_{sip\text{-}i}, P_{sip\text{-}i})$:

$$P_{mod\text{-}i} = \begin{cases} \frac{-P_{smp\text{-}i}(V-V_{smp\text{-}i})}{V_{smp\text{-}i}} + P_{smp\text{-}i} & , V < V_{smp\text{-}i} \\ P & , V_{smp\text{-}i} \le V \le V_{sip\text{-}i} \\ \frac{-P_{sip\text{-}i}(V-V_{oc})}{V_{sip\text{-}i}-V_{oc}} & , V > V_{sip\text{-}i} \end{cases} \quad (7)$$

Equation (7) is the general expression of (4) and (5) for the multi-peak case, while the resulting P_{mod1} and P_{mod2} are shown in coloured dashed line in Fig. 4 for the study-case *P-V* curve. Finally, selection of the appropriate modified curve is performed based on the flowchart of Fig. 5(b), which is essentially a general version of (6). It is worth noting that this section is included only for the sake of completeness, as the MPP estimation algorithm presented in the following is designed for the common case of two irradiance levels.

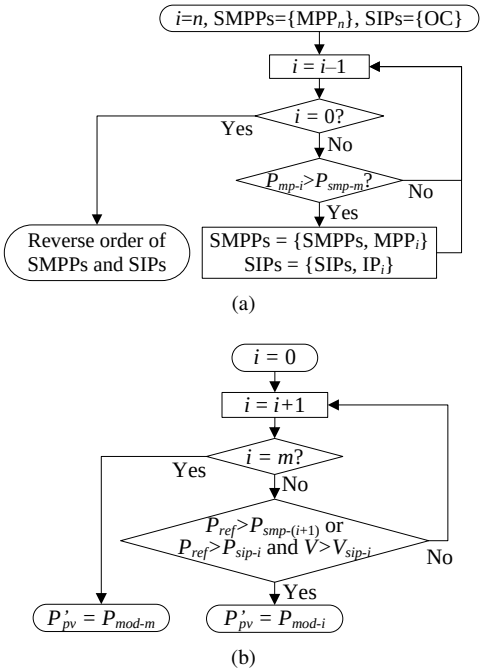

Fig. 5. Flowchart of (a) the creation of subsets SMPPs and SIPs, and (b) the selection of the appropriate modified curve.

C. MPPs Estimator Module

The two control subsystems described above require knowledge of the maximum power P_{max} and the four key operating points. To estimate these attributes while operating at a reduce power level, the concept of curve fitting presented in [13] is adopted here and expanded to partial shading conditions. An example is shown in Fig. 6: a mathematical model is fitted to a set of measurements included in a *measurement window* (green circle markers - dispersion is due to noise), in order to estimate the *P-V* curve and the key operating points (red colour). The details of this algorithm are given in Section III. The measurement window is created by deliberately introducing an oscillation of the operating point around the reference power (purple dotted line) via the Sampling & Ripple control module.

D. Sampling & Ripple Control Module

This subsystem produces the perturbation signal D_{ripple} superimposed on D_{main} (Fig. 1) in order to generate a small

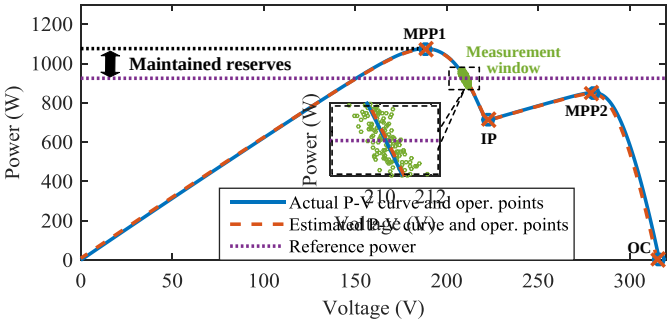

Fig. 6. Estimation of the *P-V* curve applying curve fitting on measurements.

This article has been accepted for publication in a future issue of this journal, but has not been fully edited. Content may change prior to final publication. Citation information: DOI 10.1109/TPEL.2018.2823426, IEEE Transactions on Power Electronics

operating point oscillation. This concept has been used in the past in MPPT algorithms [36], [37] and recently was employed in a power reserves control scheme [13]. According to [13], D_{ripple} is a triangular perturbation signal of fixed period t_{conv} and adjustable amplitude (see Fig. 7(a) in the following subsection). A PI controller adjusts the amplitude to regulate the measured ripple R_c to a given reference R_{cref}, as shown in Fig. 1.

In [13], the ripple metric R_c is calculated as the Euclidean distance of the boundary samples within the window, rather than simply the voltage or power ripple; this ensures constant window length on the *P-V* curve regardless of the operating region. This ripple metric works well in principle, but may lead to overestimation under high-noise conditions, when the boundary samples significantly deviate from the actual window bounds. To address this issue, this method is improved here using notch filtering techniques.

As illustrated in Fig. 1, the measured voltage V_{pv} and power P_{pv} are filtered applying notch filters at the ripple frequency f_{conv}. The induced ripple is thus filtered out from the raw signals to extract the non-oscillating $V_{pv,f}$ and $P_{pv,f}$ used in the Main control module. At the same time, the ripple components $V_{pv,r}$ and $P_{pv,r}$ are utilized in the new *curve ripple* metric introduced in this paper:

$$R_c = \sqrt{\left(\tilde{V}_{pv,r}/V_{nom}\right)^2 + \left(\tilde{P}_{pv,r}/P_{nom}\right)^2} \qquad (8)$$

where $\tilde{V}_{pv,r}, \tilde{P}_{pv,r}$ are the rms values of the ripple components and V_{nom}, P_{nom} the nominal voltage and power of the PV generator, used for normalization purposes. The new ripple metric provides reliable extraction of the induced perturbation, even in presence of strong multi-spectral noise. This fluctuation introduced in the PV output does not reach the grid side, as it is effectively filtered out by the inverter control [13].

E. Scan Module

The limited operating point oscillation induced by the Ripple control module always suffices for reliable estimation, except when the shadow first appears and its intensity is completely unknown. At that time, a much wider variation of the operating point takes place to capture the entire *P-V* curve. This procedure, commonly known as *curve scan* in the literature, is performed *only once* per shading event, triggered when the shadow extent exceeds a certain limit.

To facilitate understanding, an indicative example is shown in Fig. 7(a)-(b). Normally, the duty cycle of the converter D_{conv} (blue line in Fig. 7(a)) corresponds to the output of the Main control D_{main} (red dashed line in Fig. 7(a)) modified by the perturbation signal D_{ripple} of the Ripple control module. As a result, the PV voltage and current in Fig. 7(b) present limited fluctuation as required.

During the scan, however, the duty cycle D_{scan} is applied instead (Fig. 7(a)), which varies in a triangular manner from a very low to very high value (0 and 0.8 respectively) within a small time period t_{scan} to acquire a large part of the characteristic (not the entire curve - see voltage and current variation in Fig. 7(b)); at the last t_{rst}, the duty cycle is

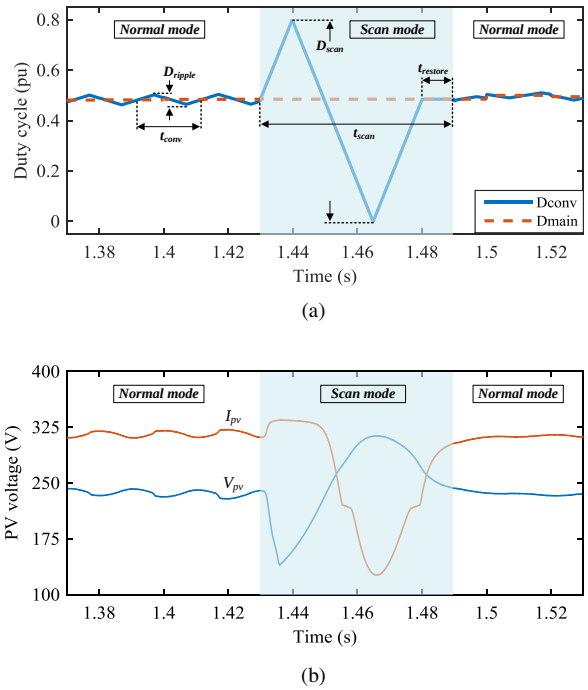

Fig. 7. Indicative example of (a) duty cycle and (b) PV voltage and current variation, according to the Scan and Ripple control modules function.

restored to its value prior to the scan in order for the system to return to its previous steady state smoothly. It is worth noting that during this process the PV power varies significantly, a power fluctuation that is inevitably reflected to the grid side to some extent. Similar short-term fluctuations are apparent in the majority of MPPT algorithms designed for partial shading conditions.

The timings t_{scan} and t_{rst} depend on hardware constraints, mainly the switching device current rating, as well as the input capacitance, cables parasitic inductance etc.; the lower these times, the shortest the duration of the scan, thus less power losses and reduced power fluctuation on the grid side. Since only a large portion of the curve is required (rather than the entire characteristic), there is no need for the operating point to converge to the OC or SC (e.g. voltage and current in Fig. 7(b) do not reach zero); this allows for very small scan timings in the range of tens of milliseconds. For the study-case system of the following sections, t_{scan} and t_{rst} can be set as low as 60 ms and 10 ms respectively (see Fig. 7(a)-(b) and Table I in Section IV). It is worth noting that the sampling frequency is high enough to capture several hundreds of measurements during this time ($t_{scan}/t_s = 60ms/50\mu s = 1200$ samples).

III. Real-Time MPP Estimation at Partial Shading

To mitigate the power losses due to partial shading, some studies introduce additional equipment or converter topology [38], [39], while others employ sophisticated MPPT algorithms in an attempt to track the global MPP on a multi-peak P-V curve [40]–[42]. During the typical MPPT function, the operating point lies fairly close to a power peak most of the time, though maybe a local one, which is very convenient for estimating purposes in model-based MPPTs (e.g. [43]). On the

This article has been accepted for publication in a future issue of this journal, but has not been fully edited. Content may change prior to final publication. Citation information: DOI 10.1109/TPEL.2018.2823426, IEEE Transactions on Power Electronics

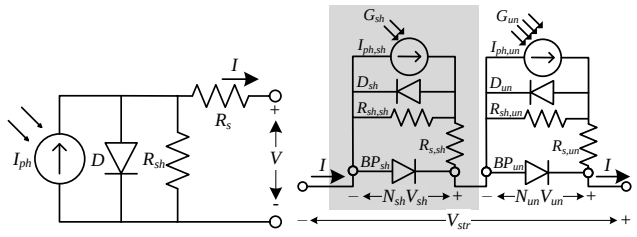

(a) (b)

Fig. 8. Equivalent circuit of the PV generator at (a) uniform illumination and (b) partial shading conditions (two different irradiance levels).

contrary, a power reserves control scheme regulates the operating point at a reduced power level, possibly not close to an MPP region; MPPs estimation under these conditions is much more challenging and requires solid theoretical background and a strong optimization algorithm.

A. Mathematical Model

1) Basic concepts: Using as a reference the shading scenario of Fig. 2(a), the four shading parameters are the effective irradiance on the unshaded part G_{un} (pu), the shade ratio s (pu), the common cell temperature T (K) and the shadow extent n_{sh} (pu). These constitute the vector of the unknowns, $x = [G_{un}, s, T, n_{sh}]^T$ ($[0.8, 0.5, 318.15, 0.167]^T$ in Fig. 2(a)), that needs to be evaluated; then, the *P-V* curve and the key operating points of the PV generator can be derived.

A PV string consists of several modules connected in series, each comprising a few cell strings; the cell string is a group of cells coupled with a bypass diode within a module, usually used as the basic modelling block in partial shading studies [27], [34], [35]. When the PV string operates under uniform illumination, its equivalent circuit is shown in Fig. 8(a) employing the single-diode PV model. When it is illuminated at two different irradiance levels, the equivalent model becomes more complicated, as in Fig. 8(b), comprising the shaded and unshaded parts, each consisting of the single-diode circuit and a bypass diode [31], [44].

2) Circuit equations: In the general case, the voltage of a cell string $V_{cs}(G,T)$ and a bypass diode $V_{bp}(G,T)$ are functions of the operating current, the effective irradiance G and the cell temperature T (detailed expressions are given in the Appendix). The PV string voltage V_{str} is the sum of the unshaded and shaded cell string voltages (Fig. 8(b)):

$$V_{str} = N_{tot}\left[(1-n_{sh})V_{un} + n_{sh}V_{sh}\right] \tag{9}$$

$$V_{un} = V_{cs}(G_{un}, T) \tag{10}$$

$$V_{sh} = \begin{cases} V_{cs}(sG_{un}, T) & , V_{sh} \geq 0 \\ V_{bp}(sG_{un}, T) & , V_{sh} < 0 \end{cases} \tag{11}$$

where N_{tot} is the total number of cell strings within the PV string and V_{un}, V_{sh} is the voltage of a single unshaded/shaded cell string. In (11), V_{sh} effectively becomes equal to the voltage drop on the conducting bypass diode when it is negative [27], [31], [34], [35]. The partial derivatives of V_{str} with respect to x are found using (9)-(11) and $\partial V_{cs}/\partial G, \partial V_{cs}/\partial T$ given in the Appendix.

3) Key operating points equations: Given the shading parameters, MPP1, MPP2, IP and OC are calculated using the following expressions [27], [29]:

$$\begin{cases} V_{mp1} = N_{tot}\left[(1-n_{sh})V_{mp}^T - n_{sh}\Delta V_D\right] \\ I_{mp1} = G_{un} I_{mp}^T \end{cases}$$
$$\begin{cases} V_{mp2} = N_{tot}\left[(1-n_{sh})\left(sV_{mp}^T + (1-s)V_{oc}^T\right) + n_{sh}V_{mp}^T\right] \\ I_{mp2} = G_{sh} I_{mp}^T\left[1 + \lambda(1-n_{sh})\right] \end{cases}$$
$$\begin{cases} V_{ip} = N_{tot}\left[(1-n_{sh})\left(sV_{mp}^T + (1-s)V_{oc}^T\right) - n_{sh}\Delta V_D\right] \\ I_{ip} = sG_{un} I_{sc}^T \end{cases}$$
$$V_{oc} = N_{tot} V_{oc}^T \tag{12}$$

where ΔV_D is the voltage drop on the bypass diode (typical values: 0.7-1.1V) and λ is an empirical coefficient (typical values: 0.03-0.06); these values could be fine-tuned on the study-case system using regression on simulation results [27]. Thereafter, the maximum power P_{max} is found as $\max\{V_{mp1}I_{mp1}, V_{mp2}I_{mp2}\}$. The terms $I_{sc}^T, V_{oc}^T, I_{mp}^T$ and V_{mp}^T refer to the cell string short-circuit current, open-circuit voltage, MPP current and MPP voltage at cell temperature T (nominal irradiance) according to [29], [30].

B. Least Squares Curve Fitting Algorithm

Objective of the curve fitting algorithm is to find the parameters vector $x = [G_{un}, s, T, n_{sh}]^T$ that optimally fits the model of Section III.A to the measurement window (Fig. 6). A widely used method for this task is the Levenberg-Marquadt algorithm, according to which the unknown vector is updated at each iteration k using [45]:

$$x^{k+1} = x^k - \left[H + \Lambda diag(H)\right]^{-1} G \tag{13}$$

where $H = J^T J$ is the Hermitian matrix, $G = J^T R$ the gradient vector, J the Jacobian matrix, R the residual vector and Λ a damping factor (here 0.001). H and G are given by:

$$G = \begin{bmatrix} s_{10001} \\ s_{01001} \\ s_{00101} \\ s_{00011} \end{bmatrix} \quad H = \begin{bmatrix} s_{20000} & s_{11000} & s_{10100} & s_{10010} \\ s_{11000} & s_{02000} & s_{01100} & s_{01010} \\ s_{10100} & s_{01100} & s_{00200} & s_{00110} \\ s_{10010} & s_{01010} & s_{00110} & s_{00020} \end{bmatrix} \tag{14}$$

where the auxiliary terms S_{xyzwr} stand for the sums of partial derivatives and residual of the n samples (V_i, I_i) within the window:

$$S_{xyzwr} = \sum_{i=1}^{n} \left(\frac{\partial V_{str}(I_i)}{\partial G_{un}}\right)^x \left(\frac{\partial V_{str}(I_i)}{\partial s}\right)^y \left(\frac{\partial V_{str}(I_i)}{\partial T}\right)^z \left(\frac{\partial V_{str}(I_i)}{\partial n_{sh}}\right)^w \left(V_{str}(I_i) - V_i\right)^r \tag{15}$$

Equation (13) is the step of the *unconstrained* optimization method. A *constrained* version of (13) is derived by imposing a limit Δx on the maximum change of x over one step:

$$x^{k+1} = x^k - \min\left\{\Delta x, \max\left\{-\Delta x, \left[H + \Lambda diag(H)\right]^{-1} G\right\}\right\} \tag{16}$$

This arises from the fact that the effective irradiance G_{un} and cell temperature T change relatively slowly [13], while

This article has been accepted for publication in a future issue of this journal, but has not been fully edited. Content may change prior to final publication. Citation information: DOI 10.1109/TPEL.2018.2823426, IEEE Transactions on Power Electronics

the shade ratio s remains almost constant for a particular shading event [46]; on the contrary, the shadow extent n_{sh} may vary from 0 to 1 within seconds. Applying an appropriate Δx limit, (16) provides more robust estimation under simultaneous changes of the shading conditions.

C. Flowchart

Since the Levenberg-Marquadt is an iterative algorithm, proper segmentation of the computational cost has to be made to permit implementation in a microcontroller (MCU). The flowchart is shown in Fig. 9, consisting of two parts: a) the *sample processing* that takes place at every sampling period $t_s = 50\mu s$ (upper part), and b) the *shading parameters update* performed once per control period $t_{conv} = 20ms$ (lower part). Thus, the measurement window length is $t_{conv}/t_s = 20ms/50\mu s = 400$ samples.

The sample processing involves all calculations made for every new sample (V_i, I_i) captured to gradually form the sum terms S_{xyzwr}. When a control period has elapsed (after 400 samples), *one iteration* (16) or (13) is performed depending on the *Mode*, in order to update x and the key operating points. In *Normal* mode, this iteration is made only when the ripple R_c is limited (not exceeding R_{cref} by more than ΔR_c), which indicates convergence to a certain power level and appropriateness of the window. The system enters *Scan* mode when the shadow extent n_{sh} first becomes more than 10% ("Shadow just appeared?" in flowchart of Fig. 9); in that case, a curve scan is performed and the entire *P-V* curve is recorded by executing unconstrained iterations till x is determined. This scan is made only *once* upon occurrence of a new shading event, rather than being executed periodically as in several MPPT algorithms; thereafter, the iterations of the algorithm in *Normal* mode suffice for adaptation to any changes in the shading conditions.

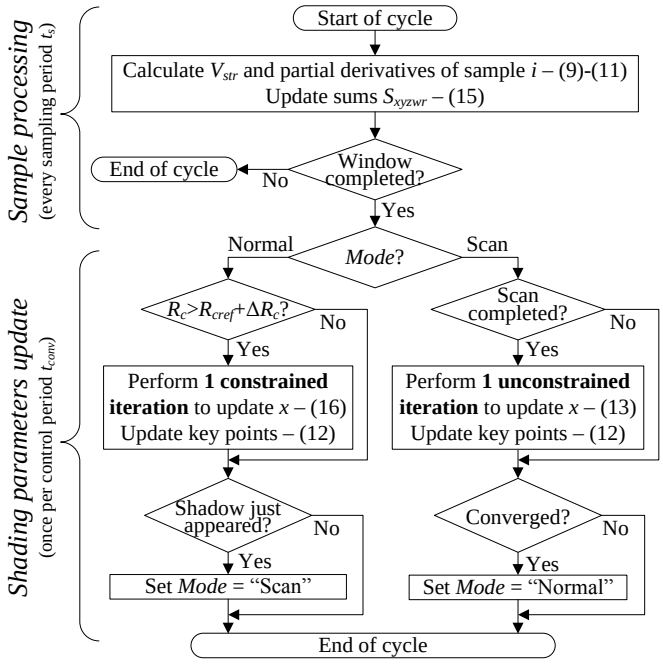

Fig. 9. Flowchart of the MPPs estimation algorithm. The upper part is executed every sampling period $t_s = 50\mu s$, whereas the lower part once per control period $t_{conv} = 20ms$.

TABLE I
CHARACTERISTICS AND PARAMETERS OF THE SIMULATED PV SYSTEM

Ratings	Value	**Timings**	Value
PV voltage V_{nom}	348 V	Sampling freq. f_s	20 kHz
PV power P_{nom}	1978 W	Control period t_{conv}	20 ms
Dc link voltage V_{dcref}	700 V	Timings t_{scan}/t_{rst}	60/10 ms
Hardware specs	Value	**Hardware specs**	Value
Dc/dc capacitance	470 μF	Dc link capacitance	1175 μF
Dc/dc inductance	600 μH	Filter inductance	20 mH
Other parameters	Value	**Estimation limits**	Value
Bp diode voltage ΔV_D	1.05 V	Max G_{un} change	100 W/m^{2}s
Empirical coefficient λ	0.03	Max T change	0.25 ^{o}C/s
Ripple reference R_{cref}	1.0%	Max s change	0.01%/s
Ripple margin ΔR_c	0.5%	Max n_{sh} change	50%/s

IV. SIMULATION RESULTS

The power circuit and control scheme of Fig. 1 is developed in MATLAB/Simulink for a 2 kW PV system. Parameter values for the system are given in Table I, corresponding also to the experimental setup of Section V. It is worth noting that the switching frequency of the inverter and boost converter are the same and equal to the sampling frequency $f_s = 20kHz$, while Space Vector Modulation (SV PWM) has been used as the inverter PWM method (see Fig. 1). In the following, step changes in the reserves command up to 40% are simulated, while the PV string experiences a hypothetical very fast shading event with simultaneous changes on effective irradiance and cell temperature. Furthermore, noise (75 SNR) is superimposed on measurements to emulate real-life conditions.

In Fig. 10(a), the achieved reserves level (blue line) sufficiently matches the requested command (red dashed line) throughout the simulation, except for short-term deviations when the scan is performed (1.5 s) and when the operating point shifts from one downhill section to another (4 and 6.7 s). A more complete picture is given in Fig. 10(b): although the maximum power (purple dashed line) varies strongly due to shading, it is estimated very accurately by the algorithm (green line); hence, the output power P_{pv} (blue line) effectively tracks its reference (red dashed line), except only for the aforementioned spikes.

The progression of the shading event is illustrated Fig. 10(c). The shadow extent n_{sh} (red dashed line) reaches 42% in a few seconds, being perfectly monitored throughout the simulation (blue line). The estimated shade ratio s (green line) becomes meaningful only after the scan at 1.5 s, coinciding thereafter with the actual s (purple dashed line). Simultaneously with the shading, the effective irradiance G_{un} and cell temperature T change by 100 W/m^2 and 1 ^{o}C respectively, as shown in in Fig. 10(d); although a small deviation between estimation and actual values does exist, this is not reflected in the estimation of P_{max} (Fig. 10(b)).

The grid-side power is illustrated in Fig. 10(e): the injected power (blue line) matches the requested value (red dashed

This article has been accepted for publication in a future issue of this journal, but has not been fully edited. Content may change prior to final publication. Citation information: DOI 10.1109/TPEL.2018.2823426, IEEE Transactions on Power Electronics

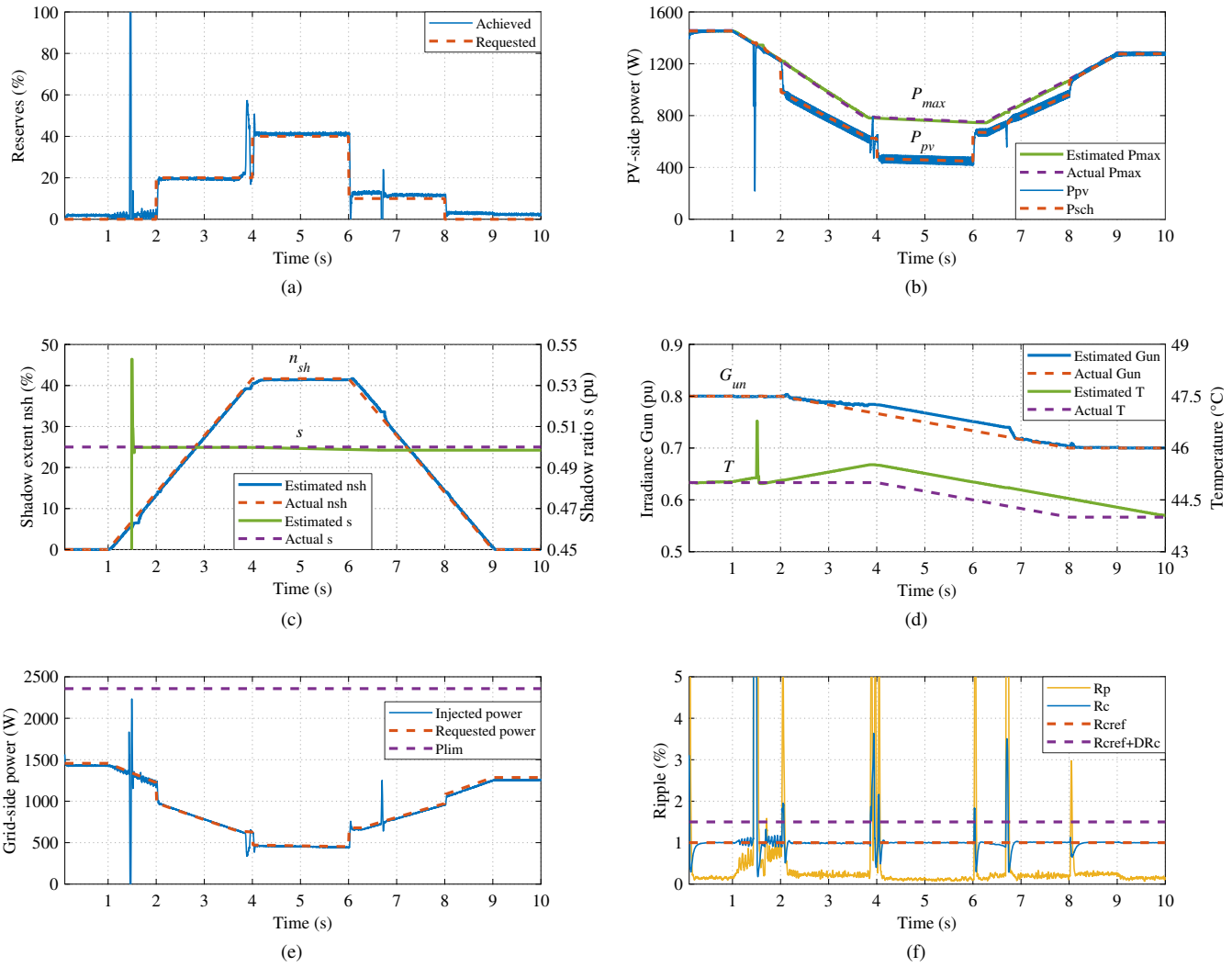

Fig. 10. Simulation results of the proposed control method for a 2 kW PV system, operating under partial shading while keeping reserves (measurement noise assumed at SNR 75). (a) Reserves, (b) PV-side output and maximum power, (c) shadow extent and intensity, (d) effective irradiance and cell temperature, (e) grid-side power, and (f) ripple.

line) (except for the discreet spikes), while the apparent ripple is negligible compared to the PV-side power ripple (blue line in Fig. 10(b)). This is better demonstrated in Fig. 10(f): the grid power ripple R_p (yellow line) varies within 0.1-0.3% most of the time, much less than the curve ripple R_c (blue line) that tracks its reference $R_{cref} = 1\%$ (red dashed line). Short-term deviations are apparent when the power reference changes abruptly, halting execution of the estimation algorithm when exceeding the purple dashed line limit.

The main conclusion is that the estimation algorithm works well even under fast simultaneous changes of irradiance and shading conditions; the grid-side power does not present noticeable high-frequency ripple, but short-term spikes are apparent when the scan is performed or the operating point switches downhill section. It is worth noting, however, that such spikes are apparent in all existing MPPTs under varying partial shading conditions, as they need to perform a scan-like variation of the operating point regularly [40]–[42] and suffer from power fluctuation when the shadow extent changes. As a matter of fact, the proposed control's spikes are normally rarer than these MPPTs, as the scan is performed only once per shading event, rather than periodically or whenever the conditions slightly change. So far, the grid operators have not imposed any restrictions to these power fluctuations, as they do not appear very often. Yet, the PV generation smoothing topic has attracted the researchers interest lately [1], [47]–[49], investigating methods to reduce the PV power variation in the general case.

V. Experimental Validation

The experimental setup used to validate the proposed control in real-life conditions consists of a 2 kW PV string comprising 12 modules connected in series (Fig. 11(a)) connected to a boost converter feeding a resistive load (Fig. 11(b)), rather than an inverter feeding the electric grid, for simplicity. The PV string is subject to outdoor solar irradiance, while the time-varying partial shading conditions are emulated by means of semi-transparent fabric that covers/uncovers the PV

This article has been accepted for publication in a future issue of this journal, but has not been fully edited. Content may change prior to final publication. Citation information: DOI 10.1109/TPEL.2018.2823426, IEEE Transactions on Power Electronics

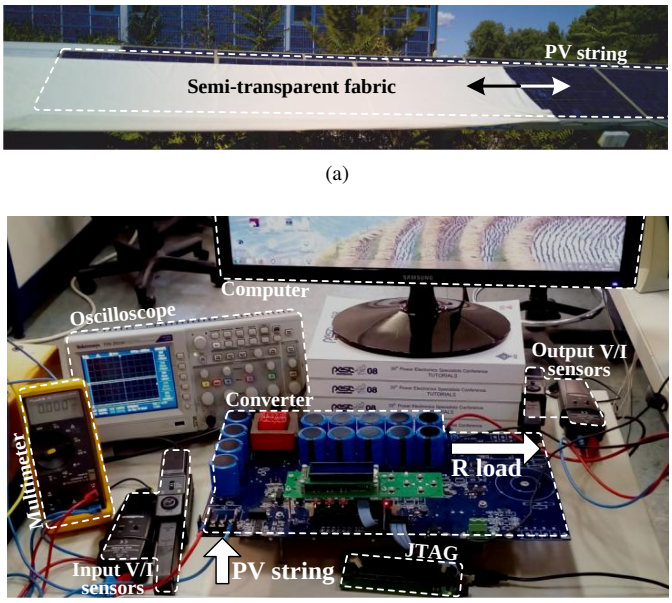

(a)

(b)

Fig. 11. Experimental setup used. (a) PV string and semi-transparent fabric, and (b) converter and measuring equipment.

TABLE II
COMPONENTS OF THE EXPERIMENTAL SETUP

Component	Details
PV string	12 x YL165 modules (165 Wp, mc-Si)
Fabric	5.5m x 1.2m fabric (32% transparency)
MCU	Texas Instr. TMS320F28335 (150MHz, 32b mult.)
Switching device	Cree C2M0080120D (1200V/36A SiC MOSFET)

string using a pulleys-ropes mechanism (Fig. 11(a)) (see also supplemental video). Main characteristics of the converter are given in Table I, with additional information provided in Table II. It is worth noting that the MCU capabilities are typical for converters of this power rating, while the firmware implemented runs smoothly, leaving the MCU idle for more than 50% of the time.

In order to test the proposed control scheme, first the parameters of the study-case system need to be determined; this is achieved by performing some special scans (*Test#1*), as explained in Section V.A. Then, on the following day (different operating conditions) the main experiment takes place (*Test#2*) to validate the power reserves control (Section V.B).

A. Test #1: Extraction of the Reference Parameters

As explained in the Appendix, in order to apply the curve fitting equations, seven coefficients must be known: the five parameters $[I_{ph0}, I_{s0}, a_0, R_{s0}, R_{sh0}]$ and the two coefficients of the two bypass diodes $[a_{bp}, I_{sbp}]$. The best way to extract these parameters is from measurements on the study-case PV system [13]. To this end, two special curve scans, denoted as reference scans, are performed to capture the *I-V* curve at uniform illumination and partial shading conditions (Fig. 12). These scans take place much more slowly (10 s in this test) for two reasons: (a) here the entire characteristic is required,

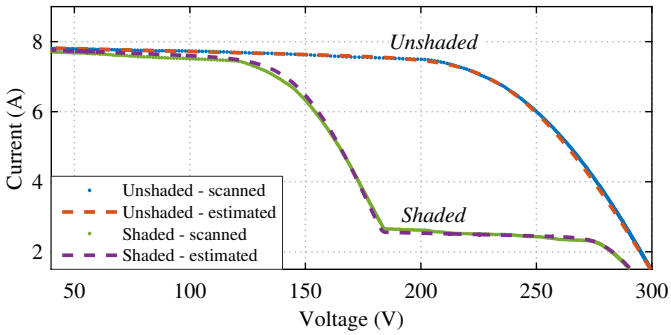

Fig. 12. Scanned *I-V* characteristics used for parameter extraction.

which entails larger duration to allow for convergence of the operating point to the OC and SC regions, and (b) there is no time restriction for the reference scans, as they are carried out very rarely (i.e. once per month or year) only to account for long-term changes on the PV system [13]. The dotted curves in Fig. 12 consists of 500 samples each.

First the five parameters are extracted from the unshaded characteristic (blue dots) using the Phangs method [13], [50]; then these are used to find the two bypass diodes' coefficients applying least squares curve fitting on the shaded curve (green dots). As shown in Fig. 12, the *I-V* characteristics reconstructed afterwards using the parameters identified (dashed lines) almost coincide with the scanned curves (dots).

The seven coefficients extracted this way are used later on as the *reference parameters* in the main experiment (*Test#2*), even though the reference conditions G_0 and T_0 differ from the STC. In other words, the MPP estimation algorithm does not really need the STC parameters; any consistent set of the seven parameters at reasonable irradiance and temperature suffice. As shown in the following section, limited inaccuracies at the identification of the reference parameters may lead to estimation errors during the normal control function, but not convergence issues or control instability.

B. Test #2: Evaluation of the Power Reserves Control

During *Test#2*, 4 out of 12 PV modules are shaded and unshaded within 30 s while the system maintains 20% reserves. This case study corresponds to a fast-moving cloud, emulated using the semi-transparent fabric (see the supplemental video for this experiment). The shading is emulated twice within a few minutes under high sun elevation and clear sky conditions: first, the power reserves control is applied and the performance is recorded; then, it is repeated while the converter simply scans the *P-V* curve at the various stages of the shading, instead of the normal control function. The measurements in the latter iteration (referred to as *actual* in the following) are used as a benchmark for the power reserves control evaluation, as the irradiance and temperature have not practically changed in such a short time period during these conditions. Since the shade ratio (fabric transparency) is known, the shadow detection part of the MPPs estimation algorithm is skipped for simplicity in this experiment.

In Fig. 13(a), operating reserves (blue line) match satisfactorily the requested level (red dashed line), with brief excursions

This article has been accepted for publication in a future issue of this journal, but has not been fully edited. Content may change prior to final publication. Citation information: DOI 10.1109/TPEL.2018.2823426, IEEE Transactions on Power Electronics

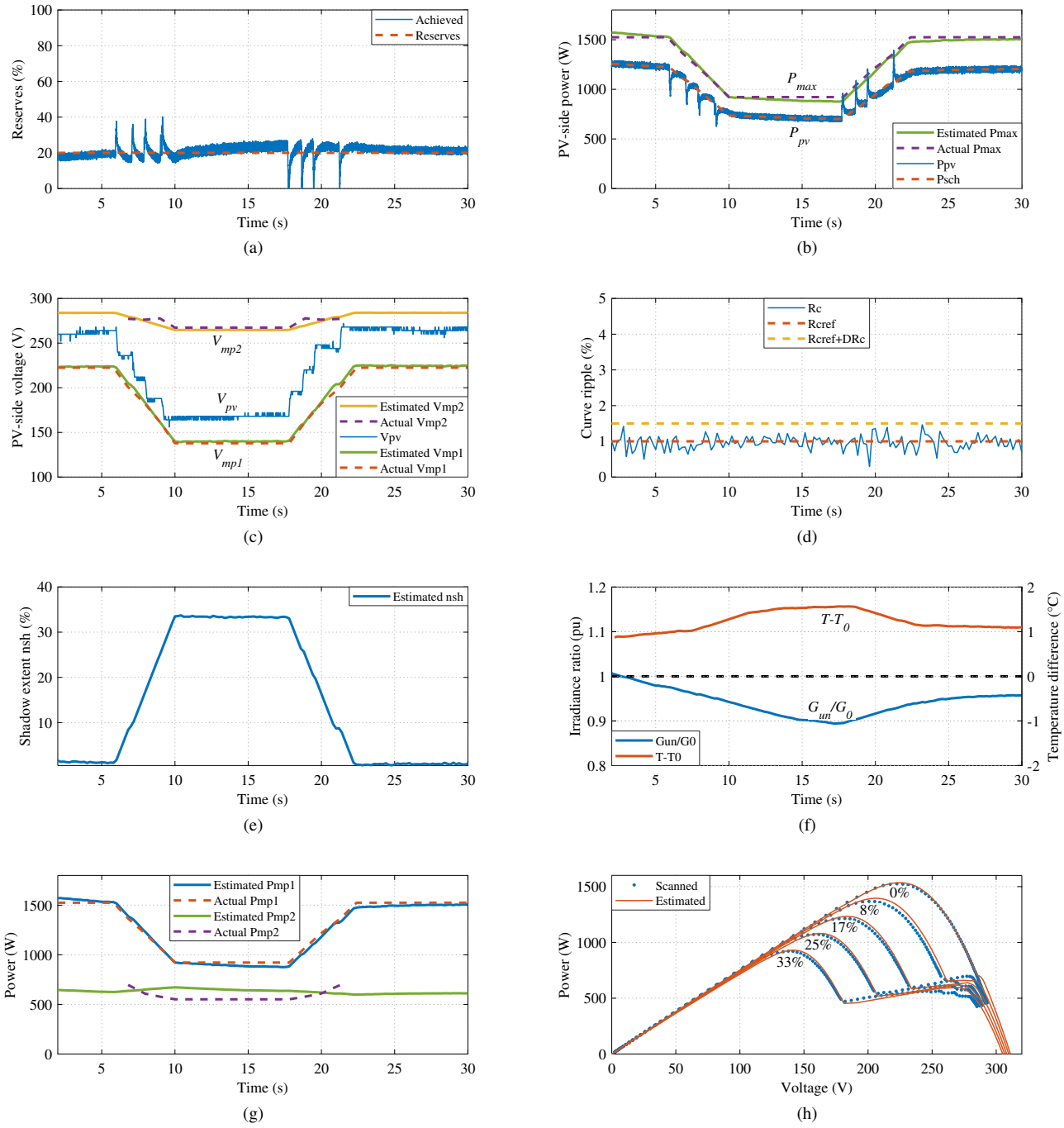

Fig. 13. Experimental results of the proposed control scheme. (a) Reserves, (b) output and maximum PV power, (c) operating MPP1 and MPP2 voltage, (d) curve ripple, (e) shadow extent, (f) irradiance and temperature, (g) MPP1 and MPP2 power, and (h) scanned and estimated P-V curves at various stages of the shading.

each time a module is shaded or unshaded due to the abrupt change of the *P-V* characteristic (one spike per module). However, these fluctuations do not reach the output of the PV system, as further explained in the following.

In Fig. 13(b), the estimated P_{max} (green line) approximates very well the actual value (purple dashed line), even though it varies significantly within a few seconds. As a result, the power at the PV side P_{pv} (blue line) tracks effectively the reference P_{sch} (red dashed line), although it still presents the aforementioned spikes. The operating voltage V_{pv} (PV side) is shown in blue colour in Fig. 13(c) along with the estimated (continuous lines) and actual (dashed lines) MPPs voltages. It is evident that V_{pv} is always between V_{mp1} and V_{mp2}, indicating operation at the leftmost downhill section of the *P-V* curve according to the modification rules of Section II.B. Both V_{mp1} and V_{mp2} estimations are quite good, while the V_{mp2} value (yellow line) is meaningless when the system is unshaded (first few and last seconds). In Fig. 13(d), the curve

This article has been accepted for publication in a future issue of this journal, but has not been fully edited. Content may change prior to final publication. Citation information: DOI 10.1109/TPEL.2018.2823426, IEEE Transactions on Power Electronics

ripple R_c (blue line) effectively tracks its reference R_{cref} (red dashed line), presenting only limited fluctuation below the yellow dashed line, thus not halting the algorithm execution at any point.

The progression of the shadow is illustrated in Fig. 13(e): the estimation algorithm keeps track of the shadow extent n_{sh} as it varies from 0% to 33% (4 shaded modules out of 12) within a few seconds. The estimated irradiance G_{un} normalized over the reference G_0 is shown in Fig. 13(f) in blue colour, ranging around 0.9-0.95; similarly, the estimated temperature T is found approximately 1-1.5 ^{o}C higher than T_0 (red line). These deviations indicate different operating conditions (*Test#2*) from the reference ones (*Test#1*), while the fluctuations on the estimations are reasonable and seem to partially counterbalance each other; as a matter of fact, this partially demonstrates the reliability of the method to a wider operating range close to the reference conditions.

In Fig. 13(g), the estimated (continuous lines) and actual (dashed lines) power of the two MPPs is illustrated; it is apparent that MPP1 is the global maximum the whole time, being monitored very accurately, whereas the weaker MPP2 is approximated with larger, albeit acceptable, error. The overall accuracy is shown in Fig. 13(h): the estimated *P-V* curves (red lines) at various stages of the shading event ($n_{sh} = 0 - 33\%$) are in good agreement with the scans performed afterwards (blue dots) over the entire operating range, confirming the wide-range capabilities of the proposed technique.

To evaluate the impact of the observed spikes, the oscillograms of the input (PV side) and output (dc link) current and power of the converter are illustrated in Fig. 14(a)-(b). The changes of the *P-V* curve along the course of the shading event are reflected mainly in the current, which experiences short-term decreases when a module is shaded and increases when it becomes unshaded (blue line in Fig. 14(a)). Yet, these spikes are significantly smoothed out at the dc link level (red line in Fig. 14(a)), as they are effectively filtered out by the inductance and capacitances of the converter. The overall effect on the power is demonstrated in Fig. 14(b): the output power (dc link - red line) proves much smoother compared to the input power (PV side blue line).

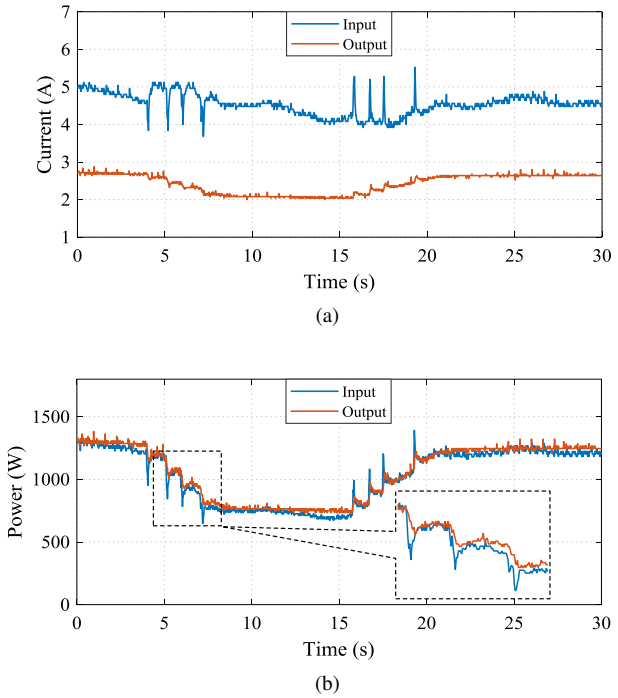

Fig. 14. Oscillograms of the input and the output (a) current and (b) power of the converter.

Overall, the experiments performed validate the effectiveness of the proposed controller applied to an actual PV system under the most demanding partial shading conditions.

VI. Conclusion

In this paper, a new control strategy for two-stage PV systems is proposed, which succeeds in maintaining operating reserves at partial shading conditions, without energy storage. The maximum power available, as well as the entire *P-V* characteristic, are estimated in real-time applying curve fitting on voltage and current measurements, dispensing thus with the need for irradiance/temperature sensors or other additional hardware. Simulation results and experimental tests on a 2 kW prototype PV system validate the accuracy and robustness of the proposed control at very fast shading events.

This is a simple way for a PV system to maintain power reserves and other ancillary services, without installing energy storage or other additional equipment. The applicability of the method to a typical PV system is verified, as it has been fully implemented in a standard MCU of moderate capabilities. Future work includes extension of the algorithm to more complicated shading scenarios of three or more irradiance levels, addressing the occasional abrupt spikes on the power output, and utilization of the reserves method in a general ancillary services control scheme with generation smoothing capabilities.

Appendix

The single-diode model shown in Fig. 8(a) involves the so-called five parameters $[I_{ph}, I_s, a, R_s, R_{sh}]$, hereafter referring to a *single cell string*. To determine these parameters, one has first to extract the reference values $[I_{ph0}, I_{s0}, a_0, R_{s0}, R_{sh0}]$ at STC and then translate them to the study-case conditions G and T, as detailed in [30]. Using the Lambert *W* function, the voltage of a cell string V_{cs} can be written as an explicit function of the current, the reference parameters and the conditions G and T [27], [30], [44]:

$$V_{cs}(G,T) = R_{sh0}\left\{I_{ph0}\left[1 + a_{Isc}(T - T_0)\right] - I/G\right\} - R_{s0}I - a_0 T/T_0 w_{cs} \quad (17)$$

$$w_{cs} = W\left\{\frac{I_{s0}R_{sh0}}{a_0}\frac{(T/T_0)^2}{G}\times e^{47.1\left(1-\frac{T}{T_0}\right)+\frac{R_{sh0}\left\{I_{ph0}\left[1+a_{Isc}(T-T_0)\right]-I/G\right\}}{a_0 T/T_0}}\right\} \quad (18)$$

where w_{cs} is an auxiliary term and the Lambert *W* function $W\{.\}$ is calculated using the series expansions provided in

[27]. Then. the partial derivatives of V_{cs} with respect to G and T are given by:

$$\frac{\partial V_{cs}(G,T)}{\partial G} = \frac{R_{sh0}I/G + a_0 w_{cs}T/T_0}{(1+w_{cs})G} \tag{19}$$

$$\frac{\partial V_{cs}(G,T)}{\partial T} = -\frac{a_0 w_{cs}}{T_0} + R_{sh0}I_{ph0}a_{Isc} - \frac{w_{cs}}{1+w_{cs}} \times \frac{(47.1+2T/T_0)a_0 + R_{sh0}\left[I_{ph0}(a_{Isc}T_0 - 1) + I/G\right]}{T} \tag{20}$$

As for the bypass diode, the derived equation involves the two coefficients a_{bp} and I_{sbp} [27]:

$$V_{bp}(G,T) = a_{bp}W\left\{\frac{I_{sbp}R_{sh0}}{a_{bp}G}e^{\frac{\left(R_{s0}+\frac{R_{sh0}}{G}\right)I - R_{sh0}I_{ph0}[1+a_{Isc}(T-T_0)]}{a_{bp}}}\right\} - \left(R_{s0}+\frac{R_{sh0}}{G}\right)I + R_{sh0}I_{ph0}[1+a_{Isc}(T-T_0)] \tag{21}$$

where the partial derivatives with respect to the operating conditions are assumed to be zero.

ACKNOWLEDGMENT

The authors would like to thank Miss Olga Schina and Mr. Anastasios Frantzeskakis for their active involvement in the experiments, and Dr. Georgios Kampitsis for developing the PV converter used.

REFERENCES

[1] C. Rahmann, V. Vittal, J. Ascui, and J. Haas, "Mitigation control against partial shading effects in large-scale PV power plants", *IEEE Trans. Sustain. Energy*, vol. 7, no. 1, pp. 173–180, Jan. 2016.

[2] E. Serban, M. Ordonez, and C. Pondiche, "Voltage and frequency grid support strategies beyond standards", *IEEE Trans. Power Electron.*, vol. 32, no. 1, pp. 298–309, Jan. 2017.

[3] Technical Guideline, "ENTSO-E network code for requirements for grid connection applicable to all generators", ENTSO-E, Mar. 2013.

[4] Y. Bae, T.-K. Vu, and R.-Y. Kim, "Implemental control strategy for grid stabilization of grid-connected PV system based on German grid code in symmetrical low-to-medium voltage network", *IEEE Trans. Energy Convers.*, vol. 28, no. 3, pp. 619–631, Sep. 2013.

[5] B.-I. Craciun, T. Kerekes, D. Sera, and R. Teodorescu, "Frequency support functions in large PV power plants with active power reserves", *IEEE J. Emerg. Sel. Top. Power Electron.*, vol. 2, no. 4, pp. 849–858, Dec. 2014.

[6] A. Hoke, E. Muljadi, and D. Maksimovic, "Real-time photovoltaic plant maximum power point estimation for use in grid frequency stabilization", in *Proc. 2015 IEEE 16th Work. Control Model. Power Electron.*, Vancouver, Jul. 2015.

[7] D. Fabozzi, N. F. Thornhill, and B. C. Pal, "Frequency restoration reserve control scheme with participation of industrial loads", in *Proc. 2013 IEEE Grenoble Conf. PowerTech*, Grenoble, Jun. 2013.

[8] D. Shin, K.-J. Lee, J.-P. Lee, D.-W. Yoo, and H.-J. Kim, "Implementation of fault ride-through techniques of grid-connected inverter for distributed energy resources with adaptive low-pass notch PLL", *IEEE Trans. Power Electron.*, vol. 30, no. 5, pp. 2859–2871, May. 2015.

[9] H.-C. Chen, C.-T. Lee, P.-T. Cheng, R. Teodorescu, and F. Blaabjerg, "A Low-Voltage Ride-Through technique for grid-connected converters with reduced power transistors stress", *IEEE Trans. Power Electron.*, vol. 31, no. 12, pp. 8562–8571, Dec. 2016.

[10] S. I. Nanou, A. G. Papakonstantinou, and S. A. Papathanassiou, "A generic model of two-stage grid-connected PV systems with primary frequency response and inertia emulation", *Electr. Power Syst. Res.*, vol. 127, pp. 186–196, Oct. 2015.

[11] A. Sangwongwanich, Y. Yang, and F. Blaabjerg, "A sensorless power reserve control strategy for two-stage grid-connected PV systems", *IEEE Trans. Power Electron.*, vol. 32, no. 11, pp. 8559–8569, Nov. 2017.

[12] A. Sangwongwanich, Y. Yang, F. Blaabjerg, and D. Sera, "Delta power control strategy for multi-string grid-connected PV inverters", *IEEE Trans. Ind. Appl.*, vol. 53, no. 4, pp. 3862–3870, Jul. 2017.

[13] E. I. Batzelis, G. E. Kampitsis, and S. A. Papathanassiou, "Power reserves control for PV systems with real-time MPP estimation via curve fitting", *IEEE Trans. Sustain. Energy*, vol. 8, no. 3, pp. 1269 – 1280, Jul. 2017.

[14] W. A. Omran, M. Kazerani, and M. M. A. Salama, "Investigation of methods for reduction of power fluctuations generated from large grid-connected photovoltaic systems", *IEEE Trans. Energy Convers.*, vol. 26, no. 1, pp. 318–327, Mar. 2011.

[15] M. Datta, T. Senjyu, A. Yona, and T. Funabashi, "A Frequency-Control Approach by Photovoltaic Generator in a PVDiesel Hybrid Power System", *IEEE Trans. Energy Convers.*, vol. 26, no. 2, pp. 559–571, Jun. 2011.

[16] G. Delille, B. Francois, and G. Malarange, "Dynamic frequency control support by energy storage to reduce the impact of wind and solar generation on isolated power system's inertia", *IEEE Trans. Sustain. Energy*, vol. 3, no. 4, pp. 931–939, Oct. 2012.

[17] X. Li, Y.-J. Song, and S.-B. Han, "Frequency control in micro-grid power system combined with electrolyzer system and fuzzy PI controller", *J. Power Sources*, vol. 180, no. 1, pp. 468–475, May. 2008.

[18] R. Tonkoski, L. Lopes, and D. Turcotte, "Active power curtailment of PV inverters in diesel hybrid mini-grids", in *Proc. 2009 IEEE Electr. Power Energy Conf.*, Montreal, QC, Oct. 2009.

[19] M. Milosevic, P. Rosa, M. Portmann, and G. Andersson, "Generation control with modified maximum power point tracking in small isolated power network with photovoltaic source", in *Proc. 2007 IEEE Power Eng. Soc. Gen. Meet.*, Tampa, FL, Jun. 2007.

[20] V. A. K. Pappu, B. Chowdhury, and R. Bhatt, "Implementing frequency regulation capability in a solar photovoltaic power plant", in *Proc. North Am. Power Symp. 2010 (NAPS 2010)*, Arlington, TX, Sep. 2010.

[21] H. Xin, Y. Liu, Z. Wang, D. Gan, and T. Yang, "A new frequency regulation strategy for photovoltaic systems without energy storage", *IEEE Trans. Sustain. Energy*, vol. 4, no. 4, pp. 985–993, Oct. 2013.

[22] H. Xin, Z. Lu, Y. Liu, and D. Gan, "A center-free control strategy for the coordination of multiple photovoltaic generators", *IEEE Trans. Smart Grid*, vol. 5, no. 3, pp. 1262–1269, May. 2014.

[23] P. Zarina, S. Mishra, and P. Sekhar, "Exploring frequency control capability of a PV system in a hybrid PV-rotating machine-without storage system", *Int. J. Electr. Power Energy Syst.*, vol. 60, pp. 258–267, Sep. 2014.

[24] E. Batzelis, T. Sofianopoulos, and S. Papathanassiou, "Active power control in PV systems using a curve fitting algorithm based on the single-diode model", in *Proc. 31st Eur. Photovolt. Sol. Energy Conf. Exhib. (EU PVSEC 2015)*, Hamburg, Sep. 2015, pp. 2402–2407.

[25] Y. Liu, L. Chen, L. Chen, H. Xin, and D. Gan, "A Newton quadratic interpolation based control strategy for photovoltaic system", in *Proc. Int. Conf. Sustain. Power Gener. Supply (SUPERGEN 2012)*, Hangzhou, Sep. 2012.

[26] E. Batzelis, S. Nanou, and S. Papathanassiou, "Active power control in PV systems based on a quadratic curve fitting algorithm for the MPP estimation", in *Proc. 29th Eur. Photovolt. Sol. Energy Conf. Exhib. (EU PVSEC 2014)*, Amsterdam, Sep. 2014, pp. 3036–3040.

[27] E. I. Batzelis, I. A. Routsolias, and S. A. Papathanassiou, "An explicit PV string model based on the Lambert W function and simplified MPP expressions for operation under partial shading", *IEEE Trans. Sustain. Energy*, vol. 5, no. 1, pp. 301–312, Jan. 2014.

[28] Y. Mahmoud and E. F. El-Saadany, "Fast power-peaks estimator for partially shaded PV systems", *IEEE Trans. Energy Convers.*, vol. 31, no. 1, pp. 206 – 217, Mar. 2015.

[29] G. N. Psarros, E. I. Batzelis, and S. A. Papathanassiou, "Partial shading analysis of multistring PV arrays and derivation of simplified MPP expressions", *IEEE Trans. Sustain. Energy*, vol. 6, no. 2, pp. 499–508, Apr. 2015.

[30] E. I. Batzelis, "Simple PV performance equations theoretically well-founded on the single-diode model", *IEEE J. Photovoltaics*, vol. 7, no. 5, pp. 1400–1409, Sep. 2017.

[31] E. Batzelis, G. E. Kampitsis, and S. A. Papathanassiou, "A MPPT algorithm for partial shading conditions employing curve fitting", in *Proc. 32th Eur. Photovolt. Sol. Energy Conf. Exhib. (EU PVSEC 2016)*, Munich, Jun. 2016, pp. 1502 – 1507.

[32] S. Manias, *Power Electronics and Motor Drive Systems*, Elsevier Science, Amsterdam, 2016.

[33] S. I. Nanou and S. a. Papathanassiou, "Modeling of a PV system with grid code compatibility", *Electr. Power Syst. Res.*, vol. 116, pp. 301–310, Nov. 2014.

[34] J. Bastidas, E. Franco, G. Petrone, C. Ramos-Paja, and G. Spagnuolo, "A model of photovoltaic fields in mismatching conditions featuring an improved calculation speed", *Electr. Power Syst. Res.*, vol. 96, pp. 81–90, Mar. 2013.

[35] M. Orozco-Gutierrez, J. Ramirez-Scarpetta, G. Spagnuolo, and C. Ramos-Paja, "A technique for mismatched PV array simulation", *Renew. Energy*, vol. 55, pp. 417–427, Jul. 2013.

[36] H.-H. Chung, K. Tse, S. Hui, C. Mok, and M. Ho, "A novel maximum power point tracking technique for solar panels using a SEPIC or Cuk converter", *IEEE Trans. Power Electron.*, vol. 18, no. 3, pp. 717–724, May. 2003.

[37] A. M. Bazzi and P. T. Krein, "Ripple correlation control: An extremum seeking control perspective for real-time optimization", *IEEE Trans. Power Electron.*, vol. 29, no. 2, pp. 988–995, Feb. 2014.

[38] M. Z. Ramli and Z. Salam, "A simple energy recovery scheme to harvest the energy from shaded photovoltaic modules during partial shading", *IEEE Trans. Power Electron.*, vol. 29, no. 12, pp. 6458–6471, Dec. 2014.

[39] F. Rong, X. Gong, and S. Huang, "A novel grid-connected PV system based on MMC to get the maximum power under partial shading conditions", *IEEE Trans. Power Electron.*, vol. 32, no. 6, pp. 4320–4333, Jun. 2017.

[40] X. Li, H. Wen, Y. Hu, L. Jiang, and W. Xiao, "Modified beta algorithm for GMPPT and partial shading detection in photovoltaic systems", *IEEE Trans. Power Electron.*, vol. 33, no. 3, pp. 2172–2186, Mar. 2018.

[41] J. Prasanth Ram and N. Rajasekar, "A novel flower pollination based global Maximum Power Point Method for solar maximum power point tracking", *IEEE Trans. Power Electron.*, vol. 32, no. 11, pp. 8486–8499, Nov. 2017.

[42] S. Lyden and M. E. Haque, "A simulated annealing Global Maximum Power Point Tracking approach for PV modules under partial shading conditions", *IEEE Trans. Power Electron.*, vol. 31, no. 6, pp. 4171–4181, Jun. 2016.

[43] J.-H. Teng, W.-H. Huang, T.-A. Hsu, and C.-Y. Wang, "Novel and fast Maximum Power Point Tracking for photovoltaic generation", *IEEE Trans. Ind. Electron.*, vol. 63, no. 8, pp. 4955–4966, Aug. 2016.

[44] E. I. Batzelis, G. E. Kampitsis, S. A. Papathanassiou, and S. N. Manias, "Direct MPP calculation in terms of the single-diode PV model parameters", *IEEE Trans. Energy Convers.*, vol. 30, no. 1, pp. 226–236, Mar. 2015.

[45] D. W. Marquardt, "An algorithm for Least-Squares estimation of nonlinear parameters", *J. Soc. Ind. Appl. Math.*, vol. 11, no. 2, pp. 431–441, Jun. 1963.

[46] E. Batzelis and S. Papathanassiou, "An efficient MPPT algorithm for partially shaded PV strings", in *Proc. 31st Eur. Photovolt. Sol. Energy Conf. Exhib. (EU PVSEC 2015)*, Hamburg, Sep. 2015, pp. 1615–1619.

[47] A. Ahmed, L. Ran, S. Moon, and J.-H. Park, "A fast PV power tracking control algorithm with reduced power mode", *IEEE Trans. Energy Convers.*, vol. 28, no. 3, pp. 565–575, Sep. 2013.

[48] H. Nazaripouya, C. Chu, H. R. Pota, and R. Gadh, "Battery energy storage system control for intermittency smoothing using optimized two-stage filter", *IEEE Trans. Sustain. Energy*, vol. 9, no. 2, pp. 664–675, Apr. 2017.

[49] M. Lei, Z. Yang, Y. Wang, H. Xu, L. Meng, J. C. Vasquez, and J. M. Guerrero, "An MPC-based ESS control method for PV power smoothing applications", *IEEE Trans. Power Electron.*, vol. 33, no. 3, pp. 2136–2144, Mar. 2018.

[50] J. C. H. Phang, D. S. H. Chan, and J. R. Phillips, "Accurate analytical method for the extraction of solar cell model paramaters", *Electron. Lett.*, vol. 20, no. 10, pp. 406–408, Jan. 1984.

Efstratios I. Batzelis (S'14-M'17) obtained the MEng degree from Technical University of Crete (TUC), Greece, and the MSc and PhD degree from National Technical University of Athens (NTUA), Greece, in 2009, 2012 and 2016 respectively, all in electrical engineering. During 2016-2017 he was a postdoctoral researcher at NTUA and Imperial College London (ICL), UK. Currently he is a Marie-Curie Research Fellow at ICL working on his project "PVCI - Photovoltaic control & integration". His current research interests include renewable energy technologies and distributed generation, especially photovoltaics, inverter and power system control.

Stavros A. Papathanassiou (S'93-M'98-SM'10) received the Diploma in Electrical Engineering in 1991 and the Ph.D. degree in 1997 from the National Technical University of Athens (NTUA), Greece. He worked for the Distribution Division of the Public Power Corporation of Greece in power quality and distributed generation studies. In 2002 he became a member of the faculty in the Electric Power Division of NTUA, where he currently serves as Professor. From 2009 to 2012 he was a member of the Board of Directors of the Hellenic TSO and Market Operator. His research mainly deals with renewable energy technologies and the integration of DG to the grid. He is a Senior Member of the IEEE and a member of CIGRE.

Bikash C. Pal (M'00-SM'02-F'13) received B.E.E. (with honors) degree from Jadavpur University, Calcutta, India, M.E. degree from the Indian Institute of Science, Bangalore, India, and Ph.D. degree from Imperial College London, London, U.K., in 1990, 1992, and 1999, respectively, all in electrical engineering. Currently, he is a Professor in the Department of Electrical and Electronic Engineering, Imperial College London. He was Editor-in-Chief of IEEE Transactions on Sustainable Energy (2012-2017) and Editor-in-Chief of IET Generation, Transmission and Distribution (2005-2012) and is a Fellow of IEEE for his contribution to power system stability and control. His current research interests include renewable energy modelling and control, state estimation, and power system dynamics.